Journal of Global Positioning Systems (2025)
Vol. 21, Issue 1: 79-97
DOI:10.5081/jgps.21.1.79

Statistical Analysis of Ionospheric Scintillation in Low-Latitude Regions

Lingqiao Zeng[1], Xiaomin Luo[1]✉, Biyan Chen[3], Wei Xiang[1], Ankang Xie[1], Jing Wang[1], Kamarul Hawari Bin Ghazali[2,4]

1. School of Geography and Information Engineering, China University of Geosciences (Wuhan), Wuhan 430079, China
2. Joint International Research Laboratory of Spatio-temporal Information and Intelligent Location Services, Guilin University of Electronic Technology, Guilin 541004, China
3. School of Geosciences and Info-Physics, Central South University, Changsha 410083, China
4. Center for Advanced Industrial Technology, University Malaysia Pahang Al Sultan Abdullah, Pekan 26600, Malaysia

✉ Corresponding authors: Xiaomin Luo, luoxiaomin@cug.edu.cn

Abstract: With the arrival of the maximum phase of Solar Cycle 25, ionospheric scintillation phenomena have become increasingly frequent, which severely impacts the capabilities of GNSS positioning, navigation, and timing services. This study collected 30-second sampling rate data from 6 GNSS stations in low-latitude regions of Asia, Oceania, the Pacific, Africa, and South America spanning the period 2014-2024. Using S_{4c} as the criterion for identifying low-latitude amplitude ionospheric scintillation, the statistical characteristics of ionospheric scintillation in various regions were analyzed. The results demonstrated a significant positive correlation between the occurrence of ionospheric scintillation in various regions and solar activity. During solar maximum years, ionospheric scintillations at the KOUG station mainly occurred in winter, spring, and autumn, while those at the other stations are predominantly observed in spring and autumn annually. Scintillation at all stations predominantly takes place between 8:00 p.m. and 2:00 a.m. local time. In low solar activity years, both the frequency and duration of ionospheric scintillation at each station decrease significantly. With the exception of the KOUG station, where scintillation remained severe, the other stations show no obvious seasonal or local time patterns. The directional distribution of ionospheric scintillation exhibits a distinct relationship with the latitude of the stations. Furthermore, the study indicates that due to the distinct meridional distribution characteristics and latitude-dependent variations of equatorial plasma bubbles, the scintillation intensity at different locations during high solar activity years follows the order from strongest to weakest: South America (near the Atlantic Ocean), Africa, the Pacific region adjacent to South America, Asia, and Oceania.

Keywords: low-latitude regions; ionospheric scintillation; spatiotemporal characteristics; solar activity

1 Introduction

The ionosphere, located at an altitude range of 60 to 1000 km above the Earth's surface, constitutes a crucial component of the Earth's atmosphere. When radio signals pass through the ionosphere, rapid and random fluctuations occur in their phase and amplitude, a phenomenon known as ionospheric scintillation. Ionospheric scintillation can be categorized into amplitude scintillation and phase scintillation [1]. Ionospheric scintillation typically occurs in low-latitude and high-latitude regions: low-latitude areas are dominated by amplitude scintillation, whereas high-latitude regions are primarily characterized by phase scintillation. Low-latitude ionospheric scintillation is mainly

caused by irregularities in the equatorial F region, with equatorial plasma bubbles (EPBs) being the primary contributing factor [2-3]. Since EPBs originate from the generalized Rayleigh-Taylor instability at the bottom of the post-sunset F layer, low-latitude ionospheric scintillation frequently occurs after sunset [3-4]. In high-latitude regions, ionospheric scintillation is primarily associated with large-scale irregular patches, which result from gradient-drift instability and the precipitation of high-energy electrons that are accelerated along geomagnetic field lines [5].

As a type of radio signal, GNSS signals also experience ionospheric scintillation when passing through the ionosphere. Ionospheric scintillation affects the quality of GNSS positioning and is currently one of the important factors leading to the degradation of GNSS positioning accuracy [6]. When amplitude and phase scintillations occur in GNSS, they restrict the coherent integration capability for weak signals and impair the normal reception and processing of signals [7]. Amplitude scintillation can reduce the signal strength below the receiver's locking threshold, making stable signal reception difficult and, in severe cases, causing interruptions in positioning services. Phase scintillation-induced Doppler frequency shifts may lead to cycle slips in GNSS carrier phase data, especially continuous cycle slips caused by intense ionospheric scintillations, which can last for several minutes. Even with the application of robust cycle slip correction algorithms, it is challenging to correct all cycle slips, thereby affecting the results of positioning using carrier phase data [8-9]. Xu et al. [10] demonstrated that during severe ionospheric scintillation, i.e., when $S_4 \geq 1$ and $\sigma_{\emptyset} \geq 1.0 rad$, the errors in GNSS precise point positioning (PPP) increase significantly. With the rapid development of autonomous driving, smart agriculture, and other fields, the demand for high-precision and stable positioning services is growing increasingly. Therefore, research on ionospheric scintillation is necessary, as it can facilitate the development of effective countermeasures to mitigate the impact of ionospheric scintillation on GNSS precise positioning [11].

With the increasing depth of research on ionospheric scintillation, current studies have preliminarily revealed the spatiotemporal patterns and physical mechanisms of ionospheric scintillation, particularly in low-latitude regions, which are typical high-incidence areas of ionospheric scintillation. In terms of spatiotemporal distribution, ionospheric scintillation events in these regions exhibit significant seasonal and local time dependencies. In terms of seasonal distribution, for example, in the East Asian region, during the vernal and autumnal equinoxes, the change in the Sun's position makes the generation of EPBs in the ionosphere more likely, resulting in scintillations that are generally more intense, frequent, and longer-lasting in spring and autumn than in summer and winter [12]. In terms of local time distribution, low-latitude ionospheric scintillation is mainly concentrated in the period from after sunset to midnight. This pattern also stems from the diurnal evolution characteristics of F-region irregularities, which (such as EPBs) typically occur during this time period. In contrast, sporadic amplitude scintillations occurring during the daytime are mostly caused by E region irregularities (e.g., the sporadic E layer), which induce ionospheric irregularities with smaller scales, leading to weaker daytime amplitude scintillations [13-14].

Despite the numerous studies conducted on the patterns of ionospheric scintillation, existing research still has certain limitations. Most findings are based on single stations or longitudinal sectors, and low-latitude scintillation research lacks cross-regional comparisons. Additionally, most studies focus on data analysis from a single year or a few years, without investigating the dynamic response of ionospheric scintillation to the solar activity cycle over an entire solar cycle. These limitations result in an insufficient comprehensive understanding of the patterns of ionospheric scintillation. Therefore, how to systematically study the patterns of ionospheric scintillation within a framework of multiple regions and long time series remains a key issue in current research.

This study aims to reveal the commonalities and

differences in scintillation patterns across various regions by analyzing ionospheric scintillation data from low-latitude areas such as Asia, Oceania, the Pacific, Africa, and South America. The research covers 11 years of data from 2014 to 2024, spanning the 24th and 25th solar activity cycles, thereby facilitating the study of long-term statistical characteristics of ionospheric scintillation. Through multi-dimensional graphical analysis, this study will explore the spatiotemporal distribution, intensity, and duration patterns of low-latitude ionospheric scintillation events, as well as their dependencies on seasons and local time.

2 Data and Methods

2.1 Construction of Scintillation Index and Definition Method of Scintillation Events

Although the indexes S_4 and $\sigma_\emptyset$ are commonly used in the study of ionospheric scintillation, the former is employed to measure the magnitude of amplitude scintillation, while the latter is used to quantify the magnitude of phase scintillation [10]. However, both indices are derived directly from the output of specialized ionospheric scintillation monitoring receivers (ISMRs). The hardware of such specialized ionospheric scintillation monitors typically requires high-precision receivers, antennas, dedicated software systems, and large storage spaces, resulting in high costs. They are only installed in certain regions, with sparse global distribution, making them unsuitable for long-term comparative studies across different low-latitude regions in this research.

To address this issue, numerous scholars have developed scintillation indices calculated using ordinary geodetic GNSS receivers, such as the indexes ROTI, AATR, and S_{4c} [15-17]. Given that amplitude scintillation predominantly occurs in low-latitude regions, the index S_{4c}, which reflects amplitude scintillation, is more appropriate for research and analysis. It is a scintillation index designed by scholars such as Luo as a substitute for the index S_4, using the C/N_0 records from ordinary receivers as the basic calculation parameter. It exhibits a very strong correlation with the index S_4, with a correlation coefficient exceeding 0.9 [17]. Its calculation formula is as follows:

$$S_{4c} = \sqrt{\frac{< SI_{\mathrm{det}}^2 > - < SI_{\mathrm{det}} >^2}{< SI_{\mathrm{det}} >^2}} \qquad (1)$$

wherein SI_{det} denotes the detrended signal intensity, and the angle brackets $\langle\rangle$ represent the arithmetic mean calculated over all observations within a 5-minute interval. SI_{det} is defined as the ratio of the signal intensity (SI) at the current epoch k to the average signal intensity over a specific time window, with its mathematical expression given as follows:

$$SI_{det} = \frac{SI(k)}{\left\langle \sum_{-\frac{n}{2}}^{1+\frac{n}{2}} SI(k+i) \right\rangle} \left(k > \frac{n}{2}\right) \qquad (2)$$

wherein n is the total number of data points within the sliding window. In this study, the sliding window duration is set to 5 minutes, so n when using 30-second data files. Assuming the noise level remains constant over a specific time period, the noise level N_0 at the current epoch k is equal to the average noise level during the aforementioned time window. By dividing the numerator of Equation (2) by $N_0(k)$ and the denominator by $\left\langle \sum_{-\frac{n}{2}}^{1+\frac{n}{2}} N_0(k+i) \right\rangle$, Equation (2) can be rewritten as follows:

$$\begin{aligned} SI_{\mathrm{det}} &= \frac{SI(k)}{N_0(k)} \cdot \frac{\left\langle \sum_{-\frac{n}{2}}^{1+\frac{n}{2}} N_0(k+i) \right\rangle}{\left\langle \sum_{-\frac{n}{2}}^{1+\frac{n}{2}} SI(k+i) \right\rangle} \\ &= \frac{\frac{SI}{N_0}(k)}{\left\langle \sum_{-\frac{n}{2}}^{1+\frac{n}{2}} \frac{SI}{N_0}(k+i) \right\rangle} (k > n/2) \end{aligned} \qquad (3)$$

wherein $SI/N_0(k)$ denotes the signal-to-noise ratio (SNR) at epoch k. It can be indirectly derived from the carrier-to-noise density ratio C/N_0 provided by GNSS RINEX format data, as expressed by $S/N_0 = 10^{0.1(C/N_0)}$. Finally, the ionospheric scintillation index S_{4c} can be calculated using Equation (1).

Due to differences in hardware design, signal tracking algorithms, and noise characteristics, GNSS

receivers of different brands (such as LEICA and TRIMBLE) exhibit significant variations in their output S_{4c} values under the same ionospheric conditions. The traditional unified threshold (e.g., 0.2) fails to adapt to multiple receivers, leading to an increase in the false alarm rate or missed detection rate of scintillation event detection. Therefore, Luo et al. [18] calculated new thresholds for different brands using the weighted average (WA) method. This threshold is constructed by integrating the advantages of the $\mu + 3\sigma$ statistical criterion and the complementary cumulative distribution function (CCDF). Studies have shown that the new WA threshold can effectively mitigate the systematic detection bias among different mainstream brand receivers. In this study, the receiver-specific thresholds calculated by Luo et al. are adopted to identify ionospheric scintillation events. It is important to note that Luo et al. only derived thresholds for mainstream GNSS receiver brands currently available on the market. A small portion of the data used in this study was collected by the ASHTECH receivers. To address the threshold issue of the ASHTECH receiver, the receiver-specific threshold calculation method proposed by Luo et al. was adopted. Using all ASHTECH data from the GLPS station during 2014–2015, the threshold for this receiver was finally calculated as 0.143.

Currently, the threshold-based detection method is widely adopted for identifying ionospheric scintillations using ground-based GNSS. Specifically, the observation data acquired by ground-based GNSS receivers are preprocessed to extract scintillation indices that characterize signal amplitude fluctuations, phase variations, or the rate of change of electron content. An ionospheric scintillation event is identified at a given observation epoch if the calculated value of the scintillation index exceeds the corresponding threshold [18]. However, this detection method is susceptible to the multipath effect, which may lead to misdetections. Satellites at low elevation angles are particularly prone to multipath interference; therefore, most studies only use data from satellites with elevation angles above 30° to mitigate the impact of multipath effects. To further reduce the influence of multipath effects and other confounding factors, Huang et al. [19], Ge et al. [20], and Cheng et al [9]. restricted their analyses to scintillation events where S_4 continuously exceeded 0.2 for at least 10 minutes or 5 minutes, respectively.

Among all stations in this study, the KAT1 station is most severely affected by multipath effects. After replacing its receiver on December 21, 2016, the multipath interference at KAT1 became prominent, with an especially severe impact in 2019. Note that, on some days in 2019, scattered data points exceeded the corresponding receiver threshold throughout the entire day. As 2019 was a solar minimum year, the overall scintillation activity throughout the year was unexpectedly higher than that in 2024 and 2014. Therefore, the 2019 data of KAT1 are excluded from subsequent analyses and discussions. Following the receiver replacement on March 2, 2020, the multipath effects at KAT1 returned to normal. Taking the KAT1 station's 2018 data as an example, the annual scatter plot shows that most S_{4c} values are below the corresponding threshold, but a large number of high-value points suddenly "spike" periodically, which occur at the same time every day and originate from the same satellite. Manual inspection confirmed that almost no genuine scintillation events occurred in 2018; however, statistical analysis of "pseudo-scintillation events" (with durations exceeding 5 minutes) revealed 2140 such events throughout the year. Among these, 58.3% lasted less than 6 minutes, 87.7% lasted less than 10 minutes, and the remaining events were scattered across durations longer than 10 minutes. Therefore, in this study, considering that these pseudo-scintillation events are mainly induced by multipath effects of low-elevation satellites, we selected only GNSS satellite measurements with elevation angles exceeding 30° during data processing to effectively mitigate multipath interference and ensure the accurate identification of ionospheric scintillation events. An ionospheric scintillation event was defined as a period where the S_{4c} index continuously exceeded the corresponding receiver threshold for more than 10 minutes. Two consecutive scintillation events separated by less than 10 minutes were

merged into a single event. For each identified event, the peak S_{4c} value and its occurrence time were recorded as the representative intensity and timing of that event [19].

2.2 Research Data

To comprehensively explore the statistical patterns of ionospheric scintillation in global low-latitude regions, this study selects 6 typical GNSS stations distributed across Asia, Oceania, the Pacific, Africa, and South America as research objects. The geographical coordinates and geomagnetic coordinates of these stations are presented in Table 1. These stations are KAT1, HKOH, KOUG, MAS1, DJIG, and GLPS. Among them, KAT1 is located in the low-latitude region of Oceania, with favorable observation coverage conditions, which can reflect the scintillation characteristics of the ionosphere in this area. HKOH is situated in southern Asia, in a region with frequent ionospheric anomaly activities, and is representative for analyzing ionospheric disturbance events in the Asian region. KOUG is located in the low-latitude region of South America, where the ionospheric structure is complex and disturbances are active, making it one of the key areas for global ionospheric research. GLPS is located in the Pacific region near South America. Both MAS1 and DJIG are situated in the low-latitude regions of Africa, and they can collaboratively reflect the typical dynamic characteristics of the ionosphere over the African continent. The aforementioned stations are widely distributed spatially, covering typical low-latitude geomagnetic environments, thus providing a solid foundation for multi-regional and multi-latitude comparative studies.

Table 1 Location of Research Stations

Station	Latitude（°）	Longitude（°）	Magnetic Latitude（°）	Magnetic Longitude（°）
DJIG	11.53N	42.85E	7.36N	116.98E
GLPS	0.74S	90.30W	8.04N	17.72W
KAT1	14.38S	132.15E	22.60S	153.76W
KOUG	5.10N	52.64W	13.70N	20.65E
MAS1	27.76N	15.63W	32.30N	61.71E
HKOH	22.25N	114.23E	12.97N	173.35W

In this study, all available 30-second observation data publicly released by the aforementioned stations through the IGS Data Center and the Lands Department of Hong Kong from 2014 to 2024 were systematically collected and processed. The relevant data cover a complete solar activity cycle (approximately 11 years), providing sufficient data support for in-depth analysis of the response relationship between ionospheric scintillation activities and solar activities. The 30-second sampling rate data were selected primarily because most data publicly available on the IGS official website during 2014–2024 are at this sampling rate, which ensures better data integrity. Zhao et al. [21-22] and Li et al. [23] have validated the applicability of 30-second sampling rate data for ionospheric scintillation detection. Furthermore, Li et al. [23] compared the S_{4c} index constructed from 30-second C/N_0 data of BeiDou-3 satellites with the standard S_4 index, revealing a high correlation coefficient of 0.95. This further confirms the reliability of the S_{4c} index calculated from 30-second sampling rate data. Meanwhile, in the latest research, Liu et al. [24] systematically compared and analyzed the S_{4c} index derived from data with sampling rates of 1 s, 5 s, 15 s, and 30 s against the S_4 index, ROTI (Rate of TEC Index), and GOLD (Global-scale Observations of the Limb and Disk) nightside images. The results demonstrated that the S_{4c} index calculated from data with different resolutions exhibits strong consistency with these scintillation metrics, particularly in capturing the variations of S_{4c} during scintillation events.

Figure 1 presents the available data of each station from 2014 to 2024, as well as the changes in the

receiver models adopted by each station during this period. During this period, various GNSS receiver devices were utilized at each station, including mainstream models such as TRIMBLE, SEPTENTRIO, LEICA, ASHTECH, and JAVAD. Additionally, the primary receiver types utilized in this study are SEPTENTRIO and LEICA, which are recognized for their high stability [18]. The other three receiver types are less frequently employed, having been used only at the DJIG and GLPS stations in selected years. It can be observed from the figure that due to factors such as data storage, the data downloaded from the IGS official website is incomplete. Therefore, in this study, if the data for a certain month is less than 20 days, the data of that month will be discarded and not included in subsequent research and discussions.

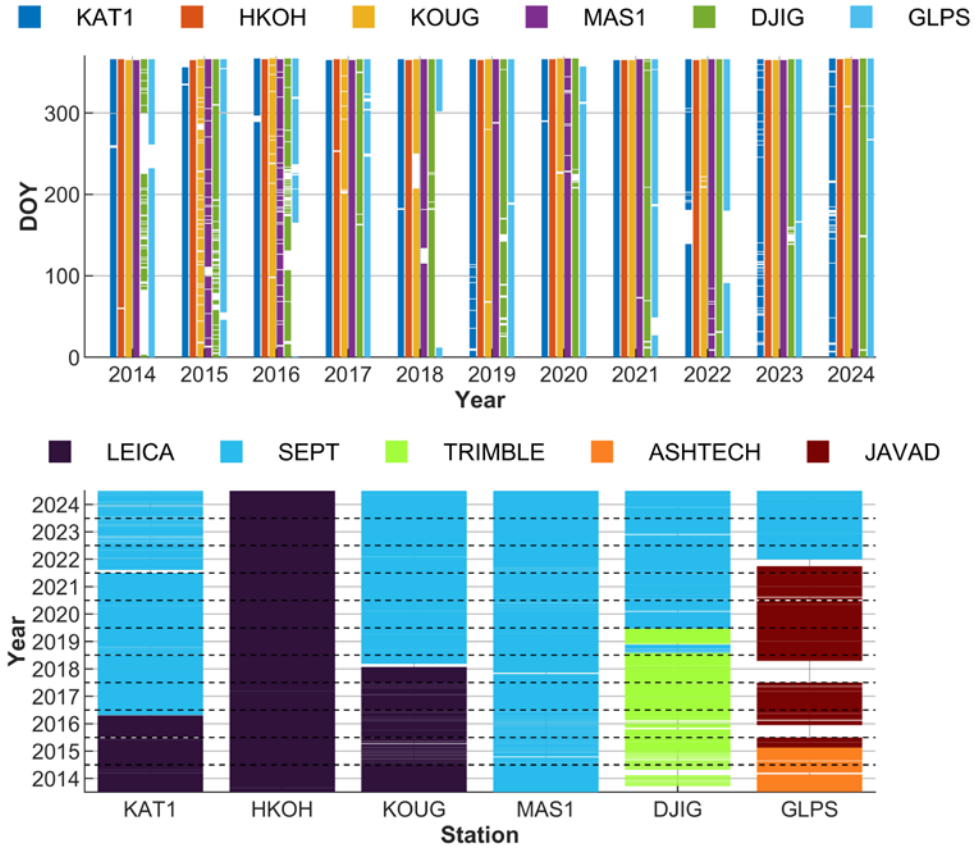

Fig. 1 Distribution of downloadable data and equipment across stations during 2014–2024. The upper subplot shows the annual downloadable data availability at each station from 2014 to 2024, with data-available periods marked by different colors (each color representing a distinct station). The lower subplot illustrates changes in receiver types at each station, where different colors correspond to different receiver models

3 Results and Discussion

3.1 Seasonal Variations of Ionospheric Scintillation

Figure 2 shows the monthly average minutes of ionospheric scintillation at 6 stations from 2014 to 2024, which is calculated by dividing the total scintillation duration occurring at the station in the month by the number of days with valid data in that month. Also included in this figure are the monthly average values of the sunspot number and F10.7 index. Figure 3 presents the monthly average number of ionospheric scintillation events at 7 stations from 2014 to 2024, calculated by dividing the total number of ionospheric scintillation events occurring at the station in the month by the number of days with data at the station in that month. In both figures, the red background indicates months with fewer than 20 days

of available data, which are excluded from the analysis and discussion.

Against the backdrop of the solar activity cycle, 2014 was in the peak phase of the 24th solar cycle, during which phenomena such as sunspot eruptions and flare activities were frequent, causing intense disturbances to the Earth's ionosphere. 2024 is projected to be the peak year of the 25th solar cycle, indicating the arrival of a new period of high solar activity. As a solar minimum, 2019 saw relatively calm solar surface conditions, with significantly reduced intensity of various activities. From 2014 to 2019, the level of solar activity showed a continuous decline, while it kept increasing from 2019 to 2024. In-depth analysis of Figures 2 and 3 reveals that, except for individual anomalies, the average ionospheric scintillation minutes and scintillation occurrence frequency at the remaining stations exhibit a positive good correlation with solar maximum years. To quantify this relationship, this study calculated the Pearson correlation coefficients between the annual daily average scintillation minutes, annual daily average scintillation counts, and the annual F10.7 Index as well as sunspot number for each year during 2014–2024, with the results presented in Table 2. The correlation coefficients for all stations exceed 0.72, while all correlation combinations for the MAS1 and HKOH stations reach above 0.9, exhibiting a strong positive correlation. These results confirm that solar activity is one of the key external driving factors governing ionospheric scintillations.

To compare the scintillation intensity across different stations, the annual daily-averaged scintillation minutes and annual daily-averaged scintillation occurrence frequency were calculated for each station. These metrics were derived by dividing the total annual scintillation minutes or occurrence frequency of each station by the number of valid days in the corresponding year, with the results plotted in Figure 4. The upper subplot presents the annual daily-averaged scintillation minutes for each station, while the lower subplot shows the annual daily-averaged scintillation occurrence frequency. Overall, during 2014–2016, the KOUG and MAS1 stations exhibited comparable levels of annual daily-averaged scintillation minutes and occurrence frequency, which were higher than those of the other four stations (with the latter four stations showing similar intensities). From 2017 to 2019, the annual daily-averaged scintillation minutes and occurrence frequency were generally consistent across all six stations. For the period 2020–2024, the KOUG station showed significantly higher scintillation intensity than the others. The second tier included the MAS1, DJIG, and GLPS stations, while the third tier consisted of the HKOH and KAT1 stations. Notably, the GLPS station’s scintillation intensity in 2024 was lower than that of the MAS1 and DJIG stations, being comparable to the third-tier HKOH and KAT1 stations. Based on geographical location comparisons, during high solar activity years, the overall scintillation intensity follows the order from strongest to weakest: South America (near the Atlantic Ocean), Africa, the Pacific region adjacent to South America, Asia, and Oceania. In contrast, the overall scintillation intensity shows no significant differences across these regions during low solar activity years.

Generally, in the Northern Hemisphere, the period from February to April is defined as spring, May to July as summer, August to October as autumn, and November to January of the following year as winter, while the opposite applies to the Southern Hemisphere. After excluding abnormal cases, it can be observed from Figures 2 and 3 that the higher the solar activity intensity, the longer the scintillation duration and the greater the number of scintillation events at each station. With the exception of the KOUG station, scintillation at other stations mainly occurs in spring and autumn. However, different from other stations, the KOUG station exhibits the longest scintillation duration and the highest number of scintillation events in winter.

The influence of solar activity on ionospheric scintillation is a complex physical process. Variations in solar activity can directly affect the heating process of the Earth's upper atmosphere, thereby altering the electron density distribution and dynamic characteristics of the ionosphere. Previous studies have demonstrated that the occurrence rate of EPBs

exhibits a systematic dependence on solar activity levels [25-26]. Huang et al. [25] utilized plasma density measurement data from multiple DMSP satellites at a local time of 19:30-21:30, in low magnetic latitude regions, and at an altitude of 840 km during 1989-2001. They found that compared with the solar maximum, the number of EPB occurrences during the solar minimum decreased by more than an order of magnitude. Tsai et al.[27] used ionospheric radio occultation observation data from FS7/COSMIC2 during 2019-2023 and found that as solar activity increased year by year from 2019 to 2023, the average occurrence rate of EPBs in low-latitude regions also increased annually. Ionospheric irregularities show an obvious pattern of variation with solar activity, which in turn leads to ionospheric scintillation exhibiting a pattern of variation with solar activity.

Tsunoda[28] found that the seasonal variation of scintillation activity is closely related to the relative position between the solar terminator and geomagnetic flux tubes. When the solar terminator is almost aligned with the geomagnetic flux tubes, ionospheric irregularities are more likely to occur, thereby enhancing scintillation activity. Nishioka et al.[29] calculated the sunset time difference between geomagnetic conjugate points to characterize the geometric relationship between geomagnetic field lines and the solar terminator. When the sunset time difference is minimized, the sunsets at the geomagnetic conjugate points are considered synchronous, a condition defined as the magnetic equinox. Their study demonstrated that magnetic equinoxes are distributed near the peaks of EPBs occurrence rates. Consistent with Nishioka's findings on the distribution of magnetic equinoxes across different longitude sectors, the seasonal patterns of scintillation distribution observed at each station in this study show good agreement: except for the Atlantic sector, where two magnetic equinoxes occur around January and November, respectively, those in other sectors are centered around March and September. Lu et al.[30] also hypothesized and validated using data from South America (2018–2024) and West Africa (2022–2024) that the alignment between the geomagnetic meridian and the sunset terminator promotes the development of ionospheric irregularities, leading to enhanced irregularity intensity and spatial extent. Consequently, the significant seasonal variation in ionospheric scintillations is attributed to the pronounced seasonal distribution of ionospheric irregularities.

Ionospheric irregularities and scintillations exhibit a strong longitudinal dependence, i.e., uneven distribution across different longitudes. Previous studies have shown that the occurrence rates of ionospheric irregularities and scintillations are higher over the Atlantic Ocean and its adjacent coastal regions (South America and Africa) than those over the Pacific Ocean and its surrounding areas[31–33]. Current explanations for this longitudinal dependence primarily focus on the longitudinal differences in post-sunset vertical plasma drifts [34–35]. As a key factor governing the generation of ionospheric irregularities [36], the vertical drift velocity exhibits significant longitudinal variations[37–38]. Zhao et al. [37] and Yizengaw et al.[38] calculated and compared the vertical drift velocities between South America and Asia, as well as between South America and Africa. Their results indicated that the vertical drift velocity over South America is higher than that over Asia and Africa, which is consistent with the ionospheric scintillation intensity observed in this study. Therefore, it is inferred that longitude sectors with higher vertical drift velocities are more conducive to the generation of ionospheric irregularities, thereby leading to the longitudinal dependence of ionospheric irregularities and scintillation distribution.

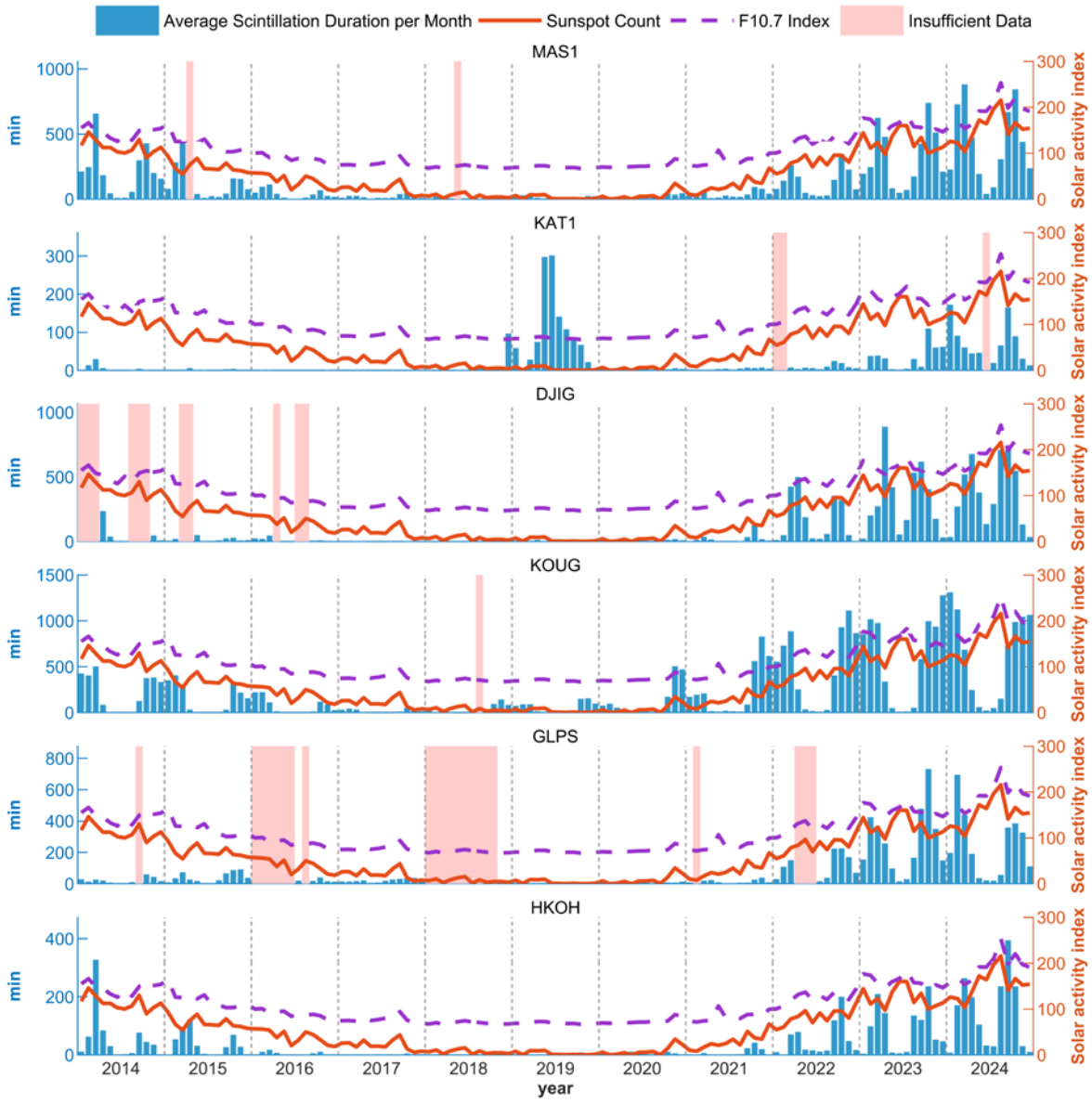

Fig. 2 Monthly daily-averaged ionospheric scintillation minutes, monthly mean sunspot number, and F10.7 index at various stations during 2014–2024. The pink-colored regions denote months with insufficient valid data (fewer than 20 observation days), which are excluded from the analysis due to inadequate data coverage. Notably, the 2019 data from the KAT1 station are excluded from the discussion

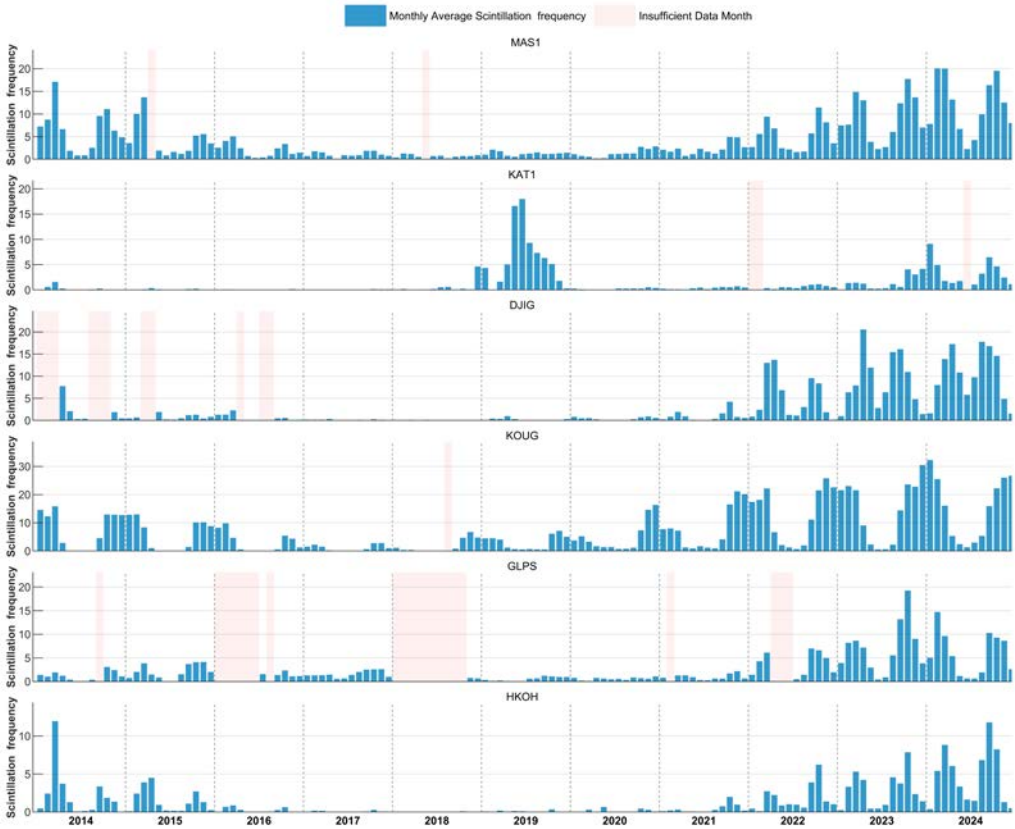

Fig.3 Monthly daily-averaged frequency of ionospheric scintillation events at various stations during 2014–2024. The pink-colored regions denote months with insufficient valid data (fewer than 20 observation days), which are excluded from the analysis due to inadequate data coverage. Notably, the 2019 data from the KAT1 station are excluded from the discussion

Table 2 Table of Pearson Correlation Coefficients Between the Annual Daily Average Scintillation Minutes, Annual Daily Average Scintillation Counts (per Station) and the Annual Daily Average of index F10.7, Sunspot Number During 2014–2024

Station	Correlation between scintillation minutes and index F10.7	Correlation between scintillation minutes and Sunspot Number	Correlation between scintillation occurrence frequency and index F10.7	Correlation between scintillation occurrence frequency and Sunspot Number
MAS1	0.979	0.963	0.991	0.978
KAT1	0.792	0.745	0.774	0.726
DJIG	0.871	0.848	0.891	0.873
KOUG	0.867	0.857	0.866	0.857
GLPS	0.833	0.814	0.832	0.824
HKOH	0.975	0.953	0.987	0.968

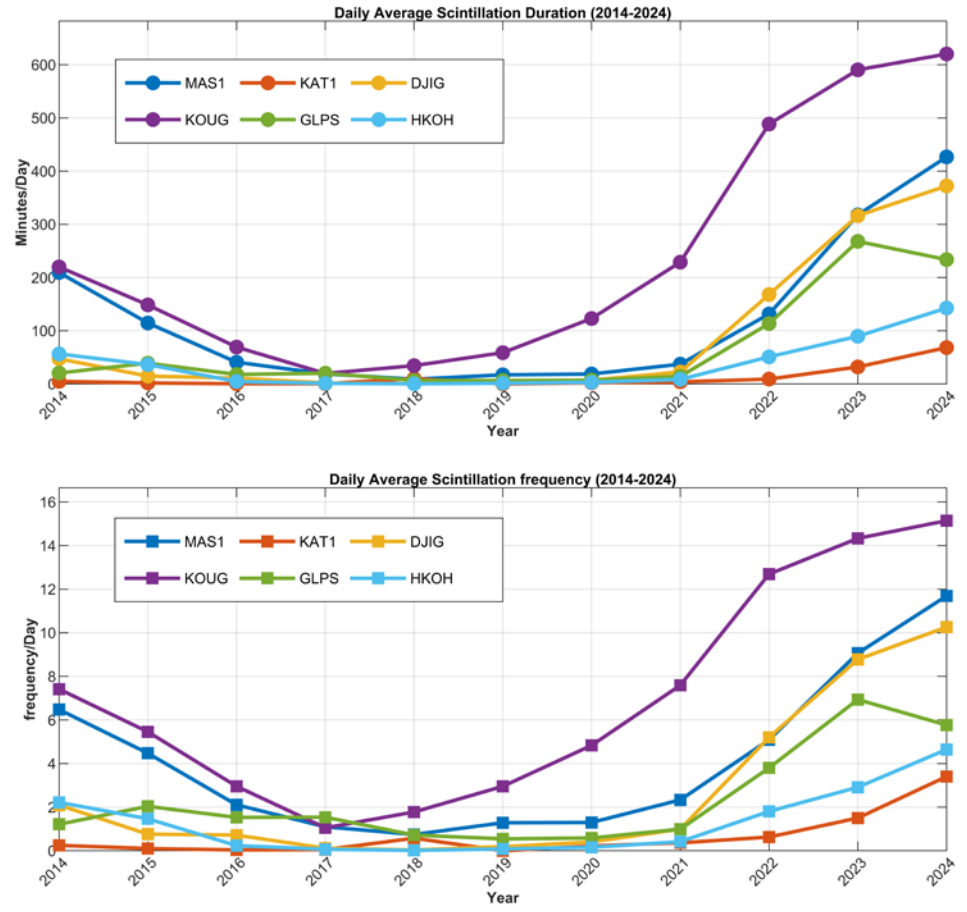

Fig. 4 Daily-averaged scintillation minutes and annual daily-averaged number of scintillation events at each station during 2014–2024. The upper subplot shows the annual daily-averaged scintillation minutes at each station, and the lower subplot presents the annual daily-averaged number of scintillation events

3.2 Local Time Variation of Scintillation Events

Figure 5 shows the 24-hour Global Positioning System Time (GPST) distribution of ionospheric scintillation events at each station from 2014 to 2024, while Figure 6 presents the monthly variation of 24-hour daily average scintillation minutes at each station during 2014–2024. Studies on the diurnal pattern of ionospheric scintillation are typically conducted based on local time. Specifically, the local time at MAS1 is approximately 1 hour behind GPST; the local time at KAT1 is approximately 9 hours ahead of GPST; the local time at DJIG is approximately 3 hours ahead of GPST; the local time at KOUG is approximately 4 hours behind GPST; the local time at GLPS is approximately 6 hours behind GPST; and the local time at HKOH is approximately 8 hours ahead of GPST.

As can be seen from Figures 5 and 6, scintillations mainly occur between 8:00 p.m. and 2:00 a.m. local time at each station. Moreover, with the increase in solar activity and the intensification of ionospheric scintillation activities, the diurnal pattern of scintillations at these stations becomes more distinct. Specifically, scintillations at MAS1 mainly occur from after 8:00 p.m. to 2:00 a.m. local time; those at KAT1 mainly occur between 7:00 p.m. and 2:00 a.m. local time; those at DJIG mainly occur between 7:00 p.m. and 2:00 a.m. local time; those at KOUG mainly occur between 7:00 p.m. and approximately 1:00 a.m. local time; those at GLPS mainly occur between 8:00 p.m. and 1:00 a.m. local time; and those at HKOH mainly occur between 8:00 p.m. and 2:00 a.m. local time.

In low-latitude regions, after sunset, the plasma density in the E region decreases more rapidly than that in the F region due to rapid recombination,

resulting in a steep density gradient at the bottom of the equatorial F region. The eastward electric field at the height of the F region in the equatorial ionosphere increases rapidly, and combined with the horizontal geomagnetic field, this causes higher-density plasma to be located above lower-density plasma. This unstable state triggers the electrostatic Rayleigh-Taylor instability, which in turn leads to the occurrence of EPBs [27, 39-40], thereby typically causing ionospheric scintillations to occur at night.

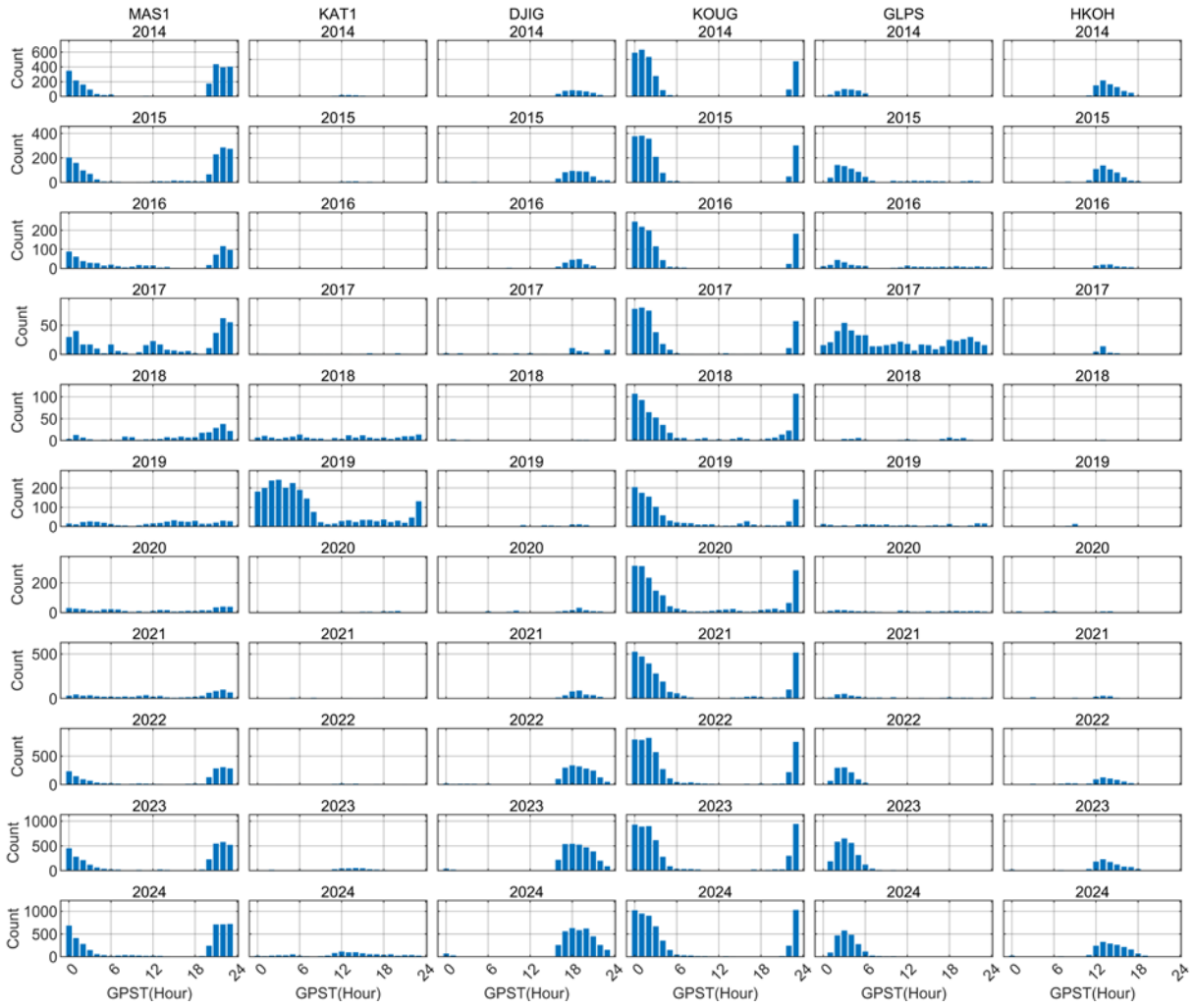

Fig. 5 Hourly number of scintillation events at each station (Global Positioning System Time, GPST) per year during 2014–2024. Each column of subplots represents a different station, and each row of subplots corresponds to a different year. Notably, the 2019 data from the KAT1 station are excluded from the discussion

Fig. 6 Heatmaps of daily-averaged scintillation minutes over 24-hour GPST per month at each station during 2014 – 2024. Each subplot corresponds to a different station, with the horizontal axis representing the years 2014 – 2024, the vertical axis denoting GPST, and different colors indicating the magnitude of scintillation minutes during the corresponding time periods. Notably, the 2019 data from the KAT1 station are excluded from the discussion

3.3 Variations in Ionospheric Scintillation Duration

The duration of ionospheric scintillation events is a key parameter for evaluating the impact of ionospheric irregularities on global navigation satellite systems (GNSS) and also serves as an important basis for studying the scale, distribution, and evolution patterns of ionospheric irregularities [41]. The size and period of ionospheric irregularities directly determine the duration of scintillation events; thus, analyzing changes in scintillation duration can provide insights into the dynamic characteristics of ionospheric irregularities. In this study, a heatmap illustrating the distribution of ionospheric scintillation event duration across local time and interannual variations is presented in Figure 7.

As shown in the figure, from 2014 to 2019, each station exhibited a consistent reduction in events with longer scintillation durations as solar activity decreased. From 2019 to 2024, events with longer scintillation durations increased continuously, and the maximum achievable duration of scintillation also gradually increased. The distribution pattern of long-duration scintillation events is highly similar to the diurnal pattern of scintillations, with such events primarily occurring around the local time window of 8:00 p.m. to 2:00 a.m. During high solar activity years, sufficient energy input and favorable ionospheric dynamic conditions facilitate the formation of larger-scale, longer-lived ionospheric irregularities. These irregularities can continuously affect satellite signals, leading to long-duration ionospheric scintillation events. This variation pattern confirms the significant regulatory role of solar activity in shaping ionospheric scintillation characteristics: solar activity not only influences the occurrence frequency of ionospheric scintillations but also exerts a critical impact on the duration of scintillation events. Large-scale ionospheric irregularities typically occur at night, a phenomenon whose physical mechanism may be closely linked to the formation, development,

and dissipation processes of ionospheric irregularities. During specific nighttime periods, the physical conditions of the ionosphere are more conducive to the generation and maintenance of large and extra-large ionospheric irregularities, thereby causing long-duration ionospheric scintillation events.

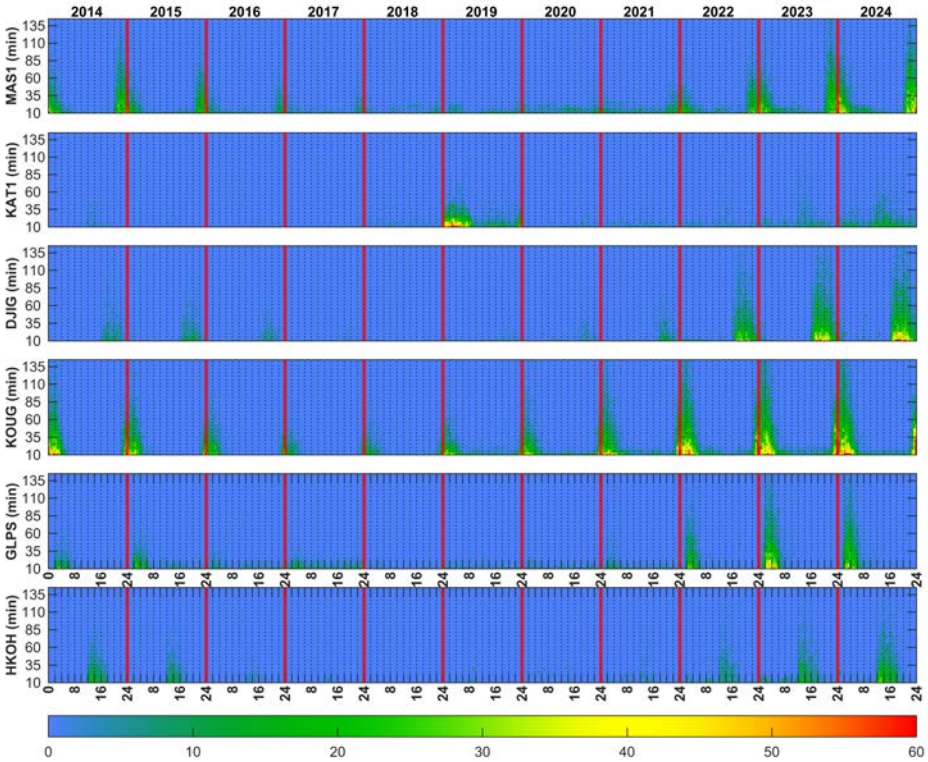

Fig. 7 Heatmaps of the interannual variation distribution of ionospheric scintillation event duration versus local time. Subplots are arranged from top to bottom corresponding to each station, with the horizontal axis representing GPST from 2014 to 2024 (binned into 30-minute intervals) and the vertical axis denoting scintillation event duration ranges (divided into 10-minute intervals). Different colors indicate the number of scintillation events in each corresponding interval. Notably, the 2019 data from the KAT1 station are excluded from the discussion

3.4 Azimuthal Patterns of Scintillation Events

In ionospheric research, the ionospheric single-shell model is commonly adopted. In this study, the ionosphere is assumed to be a single-shell model at an altitude of 450 km. Meanwhile, the observation sky above the station is divided by elevation angles into intervals of 30°–40°, 40°–50°, 50°–60°, 60°–70°, and 70°–90°. Additionally, the azimuth angles from 0° to 360° are divided into 12 sectors at 30° intervals. Through this division, the sky above the GNSS station is partitioned into 60 sub-regions. We calculated the daily average minutes of ionospheric scintillation for each interval per year at each station from 2014 to 2024, which is obtained by dividing the total scintillation minutes in the interval by the number of days with valid data in that year, as shown in Figure 8.

In general, the zonal distribution of ionospheric scintillation is closely related to the longitude and latitude of the stations. For stations near the equator, the occurrence level of ionospheric scintillation is generally high in all surrounding areas; while for stations closer to the mid-latitudes, its occurrence level is mainly concentrated in a specific direction. In the Northern Hemisphere, the occurrence level is usually the highest in the southern area, and in the Southern Hemisphere, it is the highest in the northern area. As shown in the figure, the MAS1 station, located at latitude of 27°N and magnetic latitude of 32°N, has scintillation mainly occurring in the southern region, followed by the central region, and finally the northern region. The same applies to the HKOH station, which is at latitude of 22°N and magnetic latitude of 12.97°N. The remaining four

stations, due to their lower latitudes, generally exhibit strong scintillation in all directions. Among them, the KAT1 station has little difference in scintillation intensity around it because scintillation occurs less frequently there. For the KOUG station, its scintillation is mainly concentrated in the northern and western regions; however, as the station with the highest scintillation intensity, intense scintillation occurs in all directions during high solar activity years. The DJIG station shows a significant disparity, with the intensity in the northern region being significantly greater than that in the southern region. The GLPS station, located near 0° geographic latitude and at a geomagnetic latitude of 8°N, has smaller differences in scintillation intensity across various zones compared to other stations.

Fig. 8 Directional distribution of annual daily-averaged ionospheric scintillation minutes across different azimuthal sectors at each station during 2014–2024. Each column of subplots corresponds to a different station, each row represents a different year, and different colors indicate the magnitude of annual daily-averaged ionospheric scintillation minutes in the corresponding sector. Notably, the 2019 data from the KAT1 station are excluded from the discussion

4 Conclusions

This study systematically investigated the spatiotemporal variation patterns of ionospheric scintillation in low-latitude regions across multiple regions, over a long period, using data from 6 global low-latitude GNSS stations spanning 2014–2024. The main conclusions are as follows:

(1) Regarding seasonal variations: Ionospheric scintillation is closely related to solar activity. During high solar activity years, most stations exhibit intense and frequent scintillation in spring and autumn, with weaker activity in summer and winter; during low solar activity years, the seasonal variation pattern of scintillation is less pronounced. The KOUG station, located in South America, exhibits the most intense scintillation, with the highest number of events and longest duration occurring in winter. These phenomena primarily stem from the influence of solar activity on the electron density distribution and dynamic characteristics of the ionosphere, which in turn alter the conditions for the generation of ionospheric irregularities.

(2) In terms of diurnal variations: Scintillation is mainly concentrated between 8:00 p.m. and 2:00 a.m. local time. This is because the physical conditions of the ionosphere after sunset trigger the formation of irregularities that primarily cause scintillation. Variations in scintillation duration are regulated by solar activity; as solar activity intensifies, the number of long-duration scintillation events increases significantly, and the maximum achievable duration of scintillation lengthens progressively. This reflects the impact of solar activity on the scale and lifespan of ionospheric irregularities.

(3) Regarding azimuthal distribution: Low-latitude ionospheric scintillation is correlated with the longitude and latitude of the stations. Stations closer to the equator exhibit high scintillation levels in all directions, while stations closer to mid-latitudes show scintillation concentrated in specific directions, highlighting the regional differences in the physical properties of the ionosphere.

(4) In descending order, the regions are as follows: During high solar activity years, the scintillation intensity follows the order from strongest to weakest: South America (near the Atlantic Ocean), Africa, the Pacific region adjacent to South America, Asia, and Oceania. In contrast, no significant overall differences are observed across these regions during low solar activity years. This pattern is primarily consistent with the meridional distribution of ionospheric irregularities—during high solar activity years, scintillation is more severe over South America and Africa than over Asia and Oceania.

Data Acquisition

We thank the International GNSS Service IGS (http://www.igs.gnsswhu.cn/index.php) and the Hong Kong Geodetic Survey Services (https://www.geodetic.gov.hk/tc/satref/satref.htm) for providing the GNSS data. We thank the Royal Observatory of Belgium for providing the sunspot data (Source: WDC-SILSO, Royal Observatory of Belgium, Brussels, DOI: 10.24414/qnza-ac80). Thanks to the SPDF OMNIWeb database for providing the F10.7 index data (The OMNI data were obtained from the GSFC/SPDF OMNIWeb interface at omniweb.gsfc.nasa.gov).

Acknowledgements

This study was supported by The National Natural Science Foundation of China (42274042; U25A20397), Hunan Provincial Excellent Youth Fund Project (2023JJ20060), and Joint International Research Laboratory of Spatio-temporal Information and Intelligent Location Services (C25GAH02).

Reference

[1] Crane R K. Ionospheric Scintillation[J]. Proceedings of the IEEE, 1977, 65(2): 180-199

[2] Woodman R F, La Hoz C S. Radar Observations of F Region Equatorial Irregularities[J]. Journal of Geophysical Research, 1976, 81(31): 5447 - 5466

[3] Spogli L, Piersanti M, Cesaroni C, et al. Role of the external drivers in the occurrence of low-latitude ionospheric scintillation revealed by multi-scale analysis[J]. Journal of Space Weather

and Space Climate, 2019, 9: A35.

[4] Basu B, Coppi B. Relevance of plasma and neutral wind velocities to the topology and the excitation of modes for the onset of the equatorial spread F[J]. Journal of Geophysical Research: Space Physics, 1999, 104(A1): 225-231.

[5] Jiao Y, Morton Y T. Comparison of the Effect of High-Latitude and Equatorial Ionospheric Scintillation on GPS Signals During the Maximum of Solar Cycle 24[J]. Radio Science, 2015, 50(9): 886-903

[6] Cheng J H, Cheng S X, Qi B, et al. PPP/INS Integrated Navigation Performance Analysis in Ionospheric Scintillation Environment[J]. Acta Aeronautica et Astronautica Sinica,2024,45(S1):730676

[7] Van Dierendonck A J, Klobuchar J, Hua Q. Ionospheric Scintillation Monitoring Using Commercial Single Frequency C/A Code Receivers[C]//Proceedings of ION GPS. 1993, 93: 1333-1342

[8] Shi H, Zhang D, Hao Y, et al. Modeling Study of the Effect of Ionospheric Scintillation at Low Latitudes in China[J]. Chinese Journal of Geophysics,2014,57(3):691-702

[9] Cheng J, Xu J S, Cai L. A comparison of statistical features of ionospheric scintillations and cycle slips in the mid-south region of China[J]. Chinese Journal of Geophysics, 2018, 61(1): 18-29.

[10] Xu R, Liu Z, Li M, et al. An analysis of low-latitude ionospheric scintillation and its effects on precise point positioning[J]. J Glob Position Syst, 2012, 11(1): 22-32.

[11] Li W. Study on GNSS - Based Ionospheric Anomaly Monitoring and its Application Effect[J]. Acta Geodaetica et Cartographica Sinica, 2025, 54(4):775.

[12] Ge S, Li H, Zhang S, et al. On the Properties of Lower Mid-Latitudes Ionospheric Scintillation Observed over Chengdu, China[J]. Advances in Space Research, 2024, 74(10): 4824-4834

[13] Liu K, Li G, Ning B, et al. Statistical Characteristics of Low-Latitude Ionospheric Scintillation over China[J]. Advances in Space Research, 2015, 55(5): 1356-1365

[14] Seif A, Abdullah M, Hasbi A M, et al. Investigation of Ionospheric Scintillation at UKM Station, Malaysia During Low Solar Activity[J]. Acta Astronautica, 2012, 81(1): 92-101

[15] Wu J, Zhen W, Ou M, et al. A Characterization Method of Global Ionospheric Irregularities Activities Based on GNSS Data[J]. Chinese Journal of Space Science, 2022, 42(1): 82-90

[16] Juan J M, Sanz J, Rovira-Garcia A, et al. AATR an Ionospheric Activity Indicator Specifically Based on GNSS Measurements[J]. Journal of Space Weather and Space Climate, 2018, 8: A14

[17] Luo X, Gu S, Lou Y, et al. Amplitude Scintillation Index Derived from C/N0 Measurements Released by Common Geodetic GNSS Receivers Operating at 1 Hz[J]. Journal of Geodesy, 2020, 94(2): 27

[18] Luo X, Li Y, Dai X, et al. Difference and threshold analysis of scintillation index S4c using GPS data from collocated stations at 30 s intervals during 2010–2023[J]. GPS Solutions, 2025, 29(4): 1-13.

[19] Huang L, Wang J, Jiang Y, et al. A study of GPS Ionospheric Scintillations Observed at Shenzhen[J]. Advances in Space Research, 2014, 54(11): 2208-2217

[20] Ge S, Li H, Zhang S, et al. On the properties of lower mid-latitudes ionospheric scintillation observed over Chengdu, China[J]. Advances in Space Research, 2024, 74(10): 4824-4834.

[21] Zhao D, Li W, Li C, et al. Analysis on the ionospheric scintillation monitoring performance of ROTI extracted from GNSS observations in high-latitude regions[J]. Advances in Space Research, 2022, 69(1): 142-158.

[22] Zhao D, Zhang X, Li W, et al. Extracting ionospheric phase scintillation indicator from GNSS observations with 30-s sampling interval in the high-latitude region[J]. GPS Solutions, 2023, 27(2): 79.

[23] Li Y, Luo X, Yue T, et al. Usability analysis of the amplitude scintillation index S4c derived

from BDS-3 observations[J]. Advances in Space Research, 2023, 72(11): 4868-4881.

[24] H. Liu, P. Chen, et al. Performance of ionospheric scintillation index S4c derived from geodetic GNSS observations at low latitudes: strategies and validation[J]. IEEE Geoscience and Remote Sensing Letters, 2025.

[25] Huang C Y, Burke W J, Machuzak J S, et al. Equatorial Plasma Bubbles Observed by DMSP Satellites During a Full Solar Cycle: Toward a Global Climatology[J]. Journal of Geophysical Research: Space Physics, 2002, 107(A12): SIA 7-1-SIA 7-10

[26] Vital L F R, Takahashi H, Barros D, et al. Seasonal and solar cycle dependency of relationship between equatorial plasma Bubbles and Rayleigh‐Taylor instability growth rate[J]. Space Weather, 2024, 22(10): e2024SW003959.

[27] Tsai L C, Su S Y, Schuh H, et al. Seasonal–Longitudinal Variability of Equatorial Plasma Bubbles Observed by FormoSat-7/Constellation Observing System for Meteorology Ionosphere and Climate II and Relevant to the Rayleigh–Taylor Instability[J]. Remote Sensing, 2024, 16(13): 2310

[28] Tsunoda R T. Control of the Seasonal and Longitudinal Occurrence of Equatorial Scintillations by the Longitudinal Gradient in Integrated E Region Pedersen Conductivity[J]. Journal of Geophysical Research: Space Physics, 1985, 90(A1): 447-456

[29] Nishioka M, Saito A, Tsugawa T. Occurrence characteristics of plasma bubble derived from global ground‐based GPS receiver networks[J]. Journal of Geophysical Research: Space Physics, 2008, 113(A5).

[30] Lu Y Z, Yu T, Liang Y, et al. Investigating Lifetime Characteristics of Low-Latitude Ionospheric F-Region Irregularities Using Single-Station GNSS Data[J]. Advances in Space Research, 2025, 76(11): 6041-6054

[31] Yizengaw E, Groves K M. Longitudinal and Seasonal Variability of Equatorial Ionospheric Irregularities and Electrodynamics[J]. Space Weather, 2018, 16(8): 946-968

[32] Huang C Y, Burke W J, Machuzak J S, et al. DMSP Observations of Equatorial Plasma Bubbles in the Topside Ionosphere Near Solar Maximum[J]. Journal of Geophysical Research: Space Physics, 2001, 106(A5): 8131-8142

[33] Burke W J, Huang C Y, Gentile L C, et al. Seasonal-longitudinal Variability of Equatorial Plasma Bubbles[C]//Annales geophysicae. Copernicus GmbH, 2004, 22(9): 3089-3098

[34] Huang C S. Effects of the postsunset vertical plasma drift on the generation of equatorial spread F[J]. Progress in Earth and Planetary Science, 2018, 5(1): 3.

[35] Dubazane M B, Habarulema J B. An empirical model of vertical plasma drift over the African sector[J]. Space Weather, 2018, 16(6): 619-635.

[36] Vital L F R, Takahashi H, Barros D, et al. Seasonal and solar cycle dependency of relationship between equatorial plasma Bubbles and Rayleigh‐Taylor instability growth rate[J]. Space Weather, 2024, 22(10): e2024SW003959

[37] Zhao X, Xie H, Hu L, et al. Climatology of equatorial and low-latitude F region kilometer-scale irregularities over the meridian circle around 120°E/60°W[J]. GPS Solutions, 2021, 25(1): 20.

[38] Yizengaw E, Moldwin M B, Zesta E, et al. The longitudinal variability of equatorial electrojet and vertical drift velocity in the African and American sectors[C]//Annales Geophysicae. Copernicus GmbH, 2014, 32(3): 231-238.

[39] Fejer B G, Scherliess L, De Paula E R. Effects of the Vertical Plasma Drift Velocity on the Generation and Evolution of Equatorial Spread F[J]. Journal of Geophysical Research: Space Physics, 1999, 104(A9): 19859-19869

[40] Hu L, Ning B, Li G, et al. Observations on the Field-Aligned Irregularities Using Sanya VHF Radar： 4. June Solstitial F-Region Echoes in Solar Minimum[J]. Chinese Journal of Geophysics, 2014, 57(1): 1-9

[41] Jiao Y, Morton Y T. Comparison of the Effect of High-Latitude and Equatorial Ionospheric Scintillation on GPS Signals During the Maximum of Solar Cycle 24[J]. Radio Science,

2015, 50(9): 886-903.

Authors

Lingqiao Zeng is currently a graduate student at the School of Geography and Information Engineering, China University of Geosciences (Wuhan), located in Wuhan, China. His research focuses on the impact and improvement of precise positioning under ionospheric irregularities in low-latitude regions.

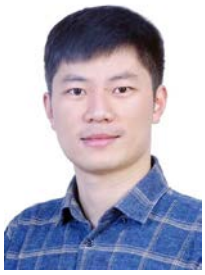

Xiaomin Luo is currently an associate professor at the School of Geography and Information Engineering, China University of Geosciences (Wuhan). He received his Ph.D. degree from the GNSS research center of Wuhan University in 2020. His current research mainly focuses on GNSS ionospheric scintillation and GNSS PPP.

Biyan Chen is currently an associate professor at Central South University. He received his Ph.D. degree from the Hong Kong Polytechnic University in 2017. His research interests include GNSS meteorology, water vapor tomography, extreme weather forecasting, and seismo-ionospheric anomalies.

Wei Xiang is currently a graduate student at the School of Geography and Information Engineering, China University of Geosciences (Wuhan), located in Wuhan, China. His research focuses on precise point positioning during magnetic storms.

Ankang Xie is currently a graduate student at the School of Geography and Information Engineering, China University of Geosciences (Wuhan), located in Wuhan, China. His research interests are RTK positioning calculation in complex ionospheric environments.

Jing Wang is currently a graduate student at the School of Geography and Information Engineering, China University of Geosciences (Wuhan), located in Wuhan, China. His current research mainly focuses on GNSS ionospheric scintillation analysis and precise point positioning (PPP).

Kamarul Hawari Bin Ghazali, Prof. Ir. Dr., is a senior academic and researcher at Universiti Malaysia Pahang Al-Sultan Abdullah (UMPSA), specializing in artificial intelligence, deep learning, machine vision, data analytics, and GNSS signal processing.